AIAA JOURNAL
Vol. 32, No. 5, May 1994

Modeling Scramjet Combustor Flowfields with a Grid Adaptation Scheme

R. Ramakrishnan* and D. J. Singh†
Analytical Services & Materials, Inc., Hampton, Virginia 23666

The accurate description of flow features associated with the normal injection of fuel into supersonic primary flows is essential in the design of efficient engines for hypervelocity aerospace vehicles. The flow features in such injections are complex with multiple interactions between shocks and between shocks and boundary layers. Numerical studies of perpendicular sonic N_2 injection and mixing in a Mach 3.8 scramjet combustor environment are discussed. A dynamic grid adaptation procedure based on the equilibration of spring-mass systems is employed to enhance the description of the complicated flow features. Numerical results are compared with experimental measurements and indicate that the adaptation procedure enhances the capability of the modeling procedure to describe the flow features associated with scramjet combustor components.

Nomenclature

A	= cell area
b_k	= biasing constants for adaptation
f_i	= mass fraction of species i
h_p	= penetration height, mm
M	= Mach number
p	= pressure
T	= temperature
t	= time
u, v	= velocity components
x	= streamwise coordinate
x_{sep}	= separation distance from slot, mm
x_{slot}	= distance measured from slot
y	= transverse coordinate
δ	= injection slot width

Subscripts

inj	= injection conditions
n	= normalized quantity
t	= total conditions
x,y	= coordinate directions
∞	= freestream conditions

Superscripts

c	= cell value
j	= coordinate directions
*	= normalized by freestream values

Introduction

THE impetus toward development of a hydrogen-fueled scramjet engine to accelerate aerospace vehicles at hypersonic speeds has focused attention on the need to accurately model compressible reacting flowfields. A great deal of effort is being directed at better understanding the effects of mixing and combustion at supersonic and hypersonic speeds. At the NASA Langley Research Center, analytical models[1,2] are being investigated for modeling mixing and reacting flows that can be validated with experimental data.

The simulation of fuel injection into a supersonic or hypersonic stream is of particular interest in efforts aimed at designing efficient scramjet combustors. In a hypersonic vehicle with a scramjet combustor, compression of the airstream begins in the inlet section; injection ramps in the throat of the engine aid in the compression and serve as fuel injector locations. The reaction caused by fuel injection proceeds in the combustor, and the combustion products are exhausted through the nozzle.

Injection of fuel into the combustion chamber can be either normal or tangential to the primary engine flow. Normal injection of fuel induces a better mixing process but creates aerodynamic choking when the inflow Mach number is low. A schematic of the flow features caused by secondary injection normal to the turbulent main flow is shown in Fig. 1. The flow features include a bow shock that forms ahead of the injector, which merges with the separation shock, and recirculation regions both upstream and downstream of the injection location. If the injectant pressure is high enough, then the interaction of the injectant with the main flow results in a Mach disk accompanied by barrel-shaped shear layers.

Various researchers have conducted numerical investigations of the mixing processes involved in perpendicular injection into a supersonic stream. Drummond[3] analyzed the perpendicular hydrogen injection from top and bottom walls in a duct that simulated the flow between two scramjet engine struts. Recent efforts in this research area include the effects of combined tangential and normal injection[4] and the use of relaxation schemes for modeling injection into supersonic crossflow.[5] A recent set of experiments by Aso et al.[6] obtained pressure data for two- and three-dimensional normal injection of N_2 into Mach 3.81 flow. A comparison of experimental measurements with a numerical analysis appears in the recent paper by Fujimori et al.[7]

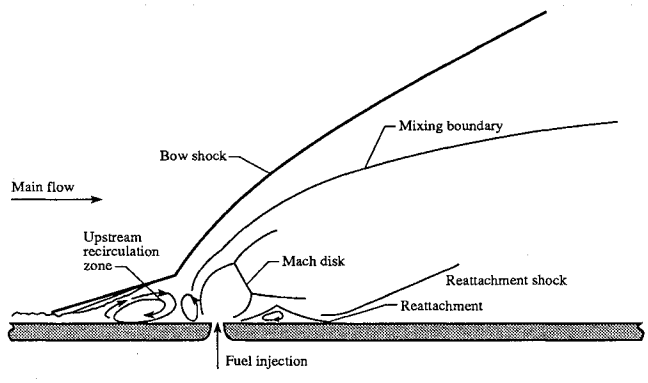

Fig. 1 Flowfield in the vicinity of injection.

Presented as Paper 93-0355 at the AIAA 31st Aerospace Sciences Meeting, Reno, NV, Jan. 11–14, 1993; received Jan. 14, 1993; revision received Nov. 16, 1993; accepted for publication Nov. 26, 1993. This paper is declared a work of the U.S. Government and is not subject to copyright protection in the United States.

*Senior Scientist, MS 159, NASA Langley Research Center, Hampton, VA 23681. Senior Member AIAA.

†Research Scientist, MS 159, NASA Langley Research Center, Hampton, VA 23681. Member AIAA.

The objective of the present study is to conduct a detailed flowfield analysis with a dynamic grid adaptation scheme for perpendicular fuel injection into a supersonic primary airstream and to evaluate the mixing processes associated with flows representative of scramjet combustors.

Governing Equations

A two-dimensional Navier-Stokes code, SPARK, is used to analyze the flowfield. The code solves the Navier-Stokes equations in conservative form with the unsplit MacCormack[8] method. In its present form, the code is formulated to model any chemically reacting flow through the use of a generalized chemistry package. In this paper, chemical reactions are modeled with a finite-rate H_2-air seven-step, seven-species reaction model.[9] An algebraic two-layer eddy viscosity model by Baldwin and Lomax[10] is used to model turbulence. Explicit details of the code structure and implementation can be found elsewhere,[11] and only a global summary is presented here.

The governing equations are transformed from the physical domain to the computational domain with an algebraic coordinate transformation. Grid velocities in the global coordinate directions are used to obtain the values of flow variables at the new grid locations after adaptation. Geometric conservation law (GCL) terms are included in the formulation to ensure that the errors caused by the rapid change in grid locations are minimized. These terms are added to the predictor and corrector steps of the unsplit MacCormack scheme.[9]

The governing equations require that boundary conditions be specified on the appropriate boundaries of the computational domain. The inflow is always supersonic, and Dirichlet boundary conditions are imposed along the $i = 1$ grid line. Specifically, pressure, temperature, u and v velocity components, and all of the species mass fractions are imposed there. At the downstream boundary the flow is also supersonic, and extrapolation boundary conditions are used to relate the downstream values to those immediately upstream. Along the solid wall, zero velocity (except at the injection locations), adiabatic surface, and zero normal pressure-gradient conditions are applied. In the injection region, the injectant velocity, pressure, temperature, and mass fractions are specified. The bottom surface is assumed to be noncatalytic; thus, the normal gradient of each species mass fraction is zero at the wall.

Initial conditions are normally prescribed for each set of calculations at all of the grid points, except at the boundaries where proper boundary conditions are imposed. Boundary conditions are applied in both the predictor and corrector steps.

Grid Adaptation Scheme

The dynamic grid adaptation procedure incorporated into the flow solver is based on the equilibration of spring-mass systems at each grid point in the finite difference mesh. A typical grid point in the interior of the domain is connected to four quadrilateral cells, and springs are imagined to be connected from the centroids of these cells to this grid point. For each grid point to be in equilibrium, the sum of the spring forces in the coordinate directions must equal zero. The aforementioned condition is valid for each grid point and is imposed throughout the domain. The grid adaptation is done in each global coordinate direction with grid adaptation constants and smoothing iterations that are independently set for each direction.

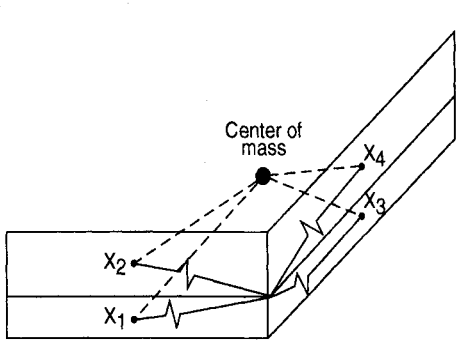

Fig. 2 Grid crossover concern in stretched grids.

The success of an adaptation procedure is largely dependent on its capability to identify regions that require adaptation. For compressible flow problems, regions that contain shocks and boundary layers must be resolved accurately. For chemically reacting flows, regions in which species concentrations change rapidly must be resolved. In this paper, adaptation measures are designed to be combinations of first derivatives of flow variables such as pressure, temperature, Mach number, and species mass fractions.

The adaptation measure or spring stiffness for each cell in the domain is written as

$$w^j = Ab_k^j |u_{k,j}|_n \tag{1}$$

where u is a flow variable and k is the summation over the number of variables used for the adaptation measure. The adaptation constants b_k are global and invariant over the grid for each coordinate direction. Spatial derivatives of the key variables are computed with bilinear interpolation functions that are defined for each quadrilateral cell. To reduce computational costs, closed-form expressions for the first derivatives at the cell nodes are used in the calculations. The cell adaptation measure is then obtained by biasing these derivatives as shown in the example:

$$e_x^c = Ab_1 \left|\frac{\partial p^c}{\partial x}\right|_n + Ab_2 \left|\frac{\partial T^c}{\partial x}\right|_n \tag{2}$$

$$e_y^c = Ab_3 \left|\frac{\partial p^c}{\partial y}\right|_n + Ab_4 \left|\frac{\partial u^c}{\partial y}\right|_n \tag{3}$$

Cell adaptation measures are normalized with respect to their maximum values, and weighting functions are taken (in, for example, the x direction) as

$$w_x^c = 1.0 + e_x^c \tag{4}$$

A smoothing procedure is used to insure a gradual change in cell sizes from a region of low grid density to one of high grid density. The cell adaptation functions are distributed to the vertices of each quadrilateral cell and then assembled again with weighting factors based on cell areas. Typically, two to three smoothing operations are done at each adaptation step.

A major concern in grid adaptation procedures is the possibility of grid-point crossover. Crossover occurs whenever the center of mass of a grid point lies outside the cells that surround it. Figure 2 shows a situation in which grid crossover is a possibility. The grid in question is surrounded by four highly stretched cells that model a compression corner. The center of mass of the grid point is located outside the boundary of the domain, which is defined by cells with centroids x_1 through x_4. This type of situation is prevalent in grids used for modeling high-speed viscous flows and must be addressed to insure a good adaptation procedure. Benson and McRae[12] use a mapping from the physical space to a parametric space to handle problems with grid crossover. The method presented in this paper modifies the adaptation stencil, which is based on physical space, to eliminate the need for coordinate transformations.

The adaptation procedure used herein generates fictitious or ghost quadrilateral cells in the coordinate directions, which form a shell that envelops the original domain. Each grid point in the original domain is assured of having the same number of cells surrounding it. The spatial coordinates of the ghost cells are obtained by linear extrapolation from the grid points that lie on the boundaries. The adaptation measures (e_x, e_y) of these cells are set equal to the cells that lie inside the boundary. The addition of ghost cells increases the size of the problem, but the relative amount of ghost cells that needs to be added decreases with increasing grid refinement. On a 101 × 81 grid, for instance, ghost cells account for 4.5% of the total cells in the domain.

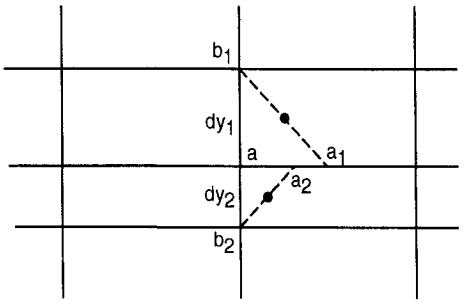

Fig. 3 Detail of local cells used for adaptation.

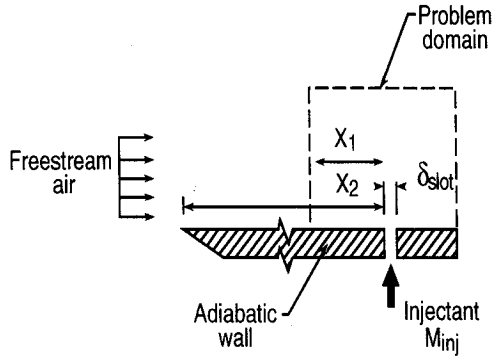

Fig. 4 Sketch of model used for perpendicular injection.

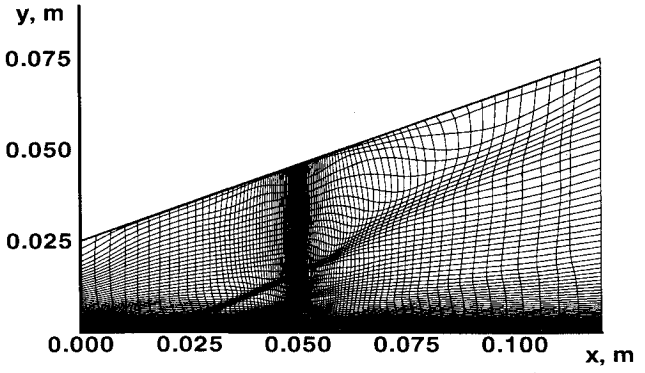

Fig. 5 Adapted grid for perpendicular injection (case 1).

The edges connected to a grid point may be part of cells that have high aspect ratios. In this case, line segments are constructed along the edges of each cell, with segments equal to the smallest edge length. Springs are assumed to be connected from a grid point to the midpoints of the line segments (for instance, a_1–b_1 and a_2–b_2 in Fig. 3) that surround it. The midpoints of these line segments must be recomputed each time the finite difference grid is moved. In practice, these calculations are done every fifth iteration during the adaptation procedure. The spring stiffness at the midpoint of a line segment is taken as the value of the adaptation measure computed for the associated cell.

The use of ghost cells on boundaries and locally defined centroids on each cell corner insures an adaptation scheme that does not require different adaptation stencils for the interior and sides of a domain. The procedure can be employed with highly stretched grids so that the problem of grid crossover is prevented. Further details of the adaptation procedure can be found in Ref. 13.

Results and Discussion

A sketch of the model considered for perpendicular injection of N_2 into a supersonic airstream is shown in Fig. 4. The slot width, injectant fluid, and injection conditions for the various cases that will be discussed are shown in Table 1.

Case 1: $\delta = 0.5$ mm

The primary flow of air is assumed to be at Mach 3.81 at a total pressure and temperature of $1.2e + 06$ Pa and 283 K, respectively. Nitrogen is injected into the test section normal to the surface at Mach 1 at a total pressure of $0.6e + 06$ Pa and total temperature of 283 K and is pumped in through an orifice that is 0.5-mm wide. A fully developed turbulent profile is imposed at the inflow boundary at each time step.

A 101×81 mesh is employed with the grid stretched in the normal direction to model the turbulent boundary layer. Grid points are also clustered in the streamwise direction at the injection location ($x = x_1$ in Fig. 4) to define the flow physics near the injection region. The finite difference grid is adapted to enhance the definition of regions with sharp gradients such as shocks and shear layers. At the end of 8000 local time steps, the grid adaptation scheme is utilized every 1000 time steps to move gird points to regions of large gradients. The dynamic grid adaptation procedure is used for the next 100 global time steps; flow variables are reinterpolated with grid velocity terms. The computational expense involved in invoking the grid adaptation procedure at regular intervals can be quantified by comparing typical run times for a sample problem; an analysis without any adaptation took 2300 s on a Cray Y-MP, whereas an analysis with grid adaptations took 2560 s.

Grid adaptation measures are based on combinations of Mach number and density gradients in both coordinate directions. Re-

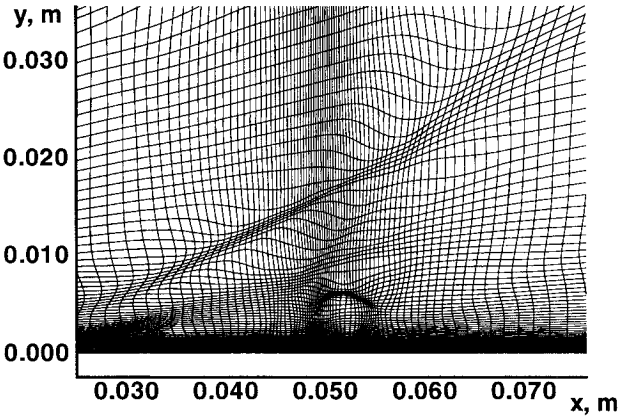

Fig. 6 Detail of adapted mesh near injection location.

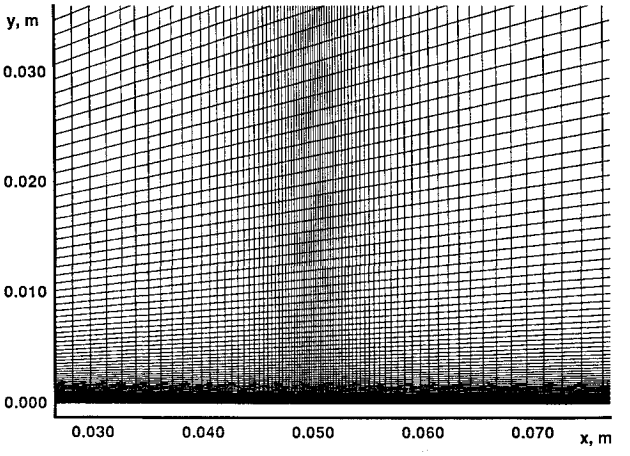

Fig. 7 Detail of unadapted mesh near injection location.

Table 1 Normal injection cases

Case	Injectant	δ_{slot}, mm	P^*_{inj}
1	Nitrogen	0.5	31.00
2	Nitrogen	1.0	9.76
3	Nitrogen	1.0	19.70
4	Nitrogen	1.0	29.74

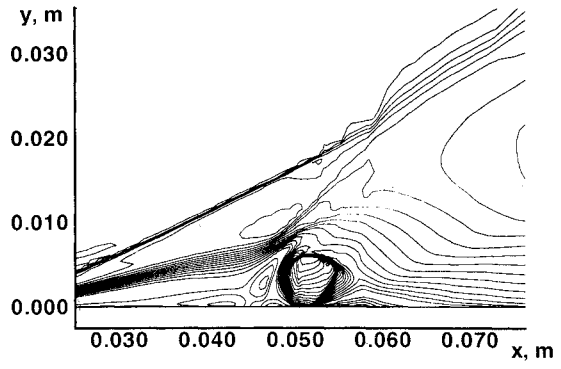

Fig. 8 Mach number contours near injection location.

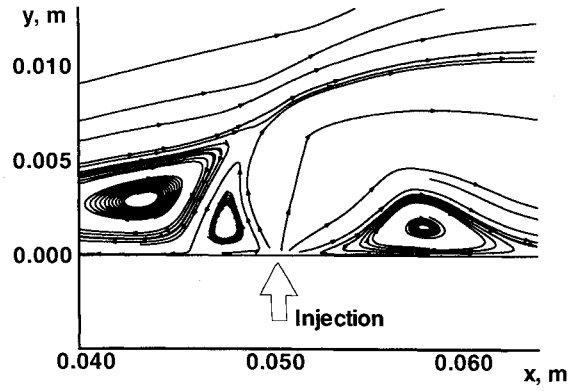

Fig. 9 Streamlines near injection location.

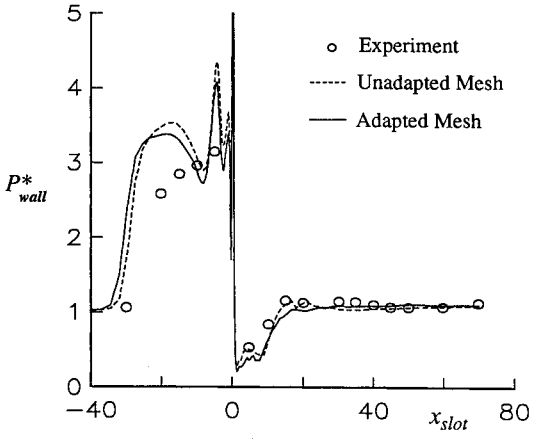

Fig. 10 Surface pressure distribution for case 1.

peated grid adaptations are performed until the relative change in grid locations from one adaptation to another decreased below a preset threshold level. The presence of the separation bubble and reattachment regions in the vicinity of injection caused the global residuals to drop only two orders of magnitude. In the cases discussed in this paper, convergence is based on the realization of an unchanged wall pressure distribution.

The grid obtained after multiple adaptations appears in Fig. 5, and the adapted and unadapted grids in the vicinity of the N_2 injection appear in Figs. 6 and 7, respectively. The adaptation procedure moves grid points to regions in the flowfield that contain large gradients. The Mach number contours in Fig. 8 show the bow shock induced by the flow blockage from the N_2 injection, and this shock causes the flow approaching the injection location to separate, which produces the separation shock. The results of the adaptation to the shock can be seen in Fig. 8. The injectant, at a higher pressure than the freestream, expands as it exits the slot, and equilibration of the injectant pressure and the pressure behind the bow shock causes a normal shock to form just ahead of injection. This surface (called a Mach disk in a three-dimensional flow) and barrel-shaped shear layers are clearly defined in the contours of Fig. 8. The separated flow region ahead of the injection station is also evident in the Mach number contours.

Streamlines in Fig. 9 indicate the complex nature of the flowfield in the vicinity of the N_2 injection. A study of the species mass fractions (not shown herein) indicates that the mixing process is essentially confined to the upper boundary between the primary flow and the injectant. The presence of one clockwise- and one counterclockwise-rotating vortex ahead of the injection point and a clockwise-rotating vortex behind it is also clearly evident in Fig. 9.

The distribution of pressure along the adiabatic wall for the unadapted and adapted grids are compared with the experimental measurements of Aso et al.[6] in Fig. 10. Wall pressures are normalized with respect to the freestream pressure of the primary flow and plotted as a function of the distance from the slot. The numerical results show a hump in the wall pressure as the flow approaches the injection station and two peaks in pressure that correspond to spurious oscillations caused by insufficient control of

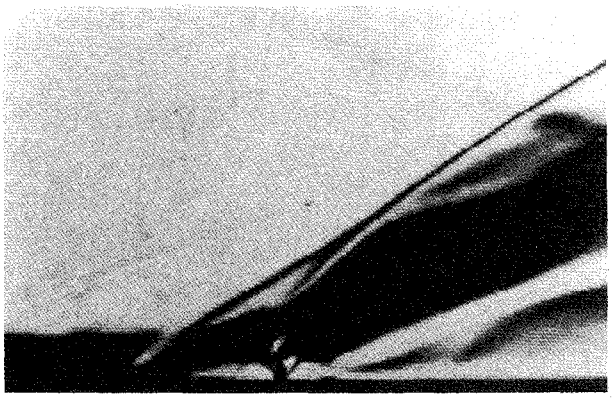

Fig. 11 Experimental schlieren photograph for case 2.

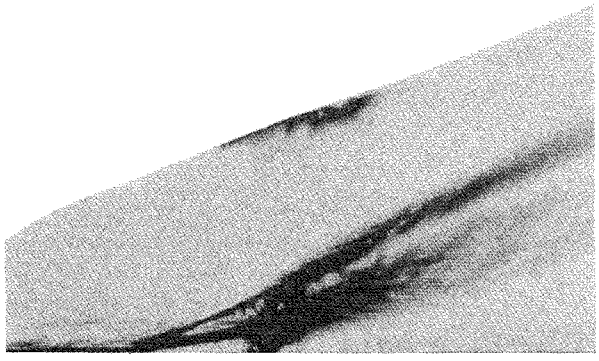

Fig. 12 Numerical schlieren for case 2.

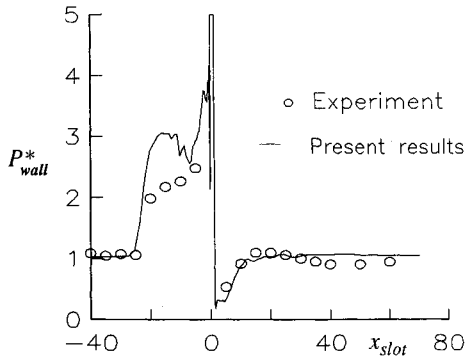

Fig. 13 Surface pressure distribution for case 2.

numerical dissipation. The unadapted grid shows a larger peak in the pressure just ahead of injection as well as a higher pressure hump well ahead of the injection location compared with the adapted grid. Other computational results[7,14] in recent literature for normal injection also report the sharp pressure peaks just ahead of the injection location. Downstream of the injection the comparison between the computational results and experimental data is quite good.

One of the disadvantages of the Baldwin-Lomax turbulent model is that it uses spatial lengths as a basis for calculating turbulent viscosity, and these measures are unavailable for regions wherein separation and reattachment occur. This leads to inaccuracies in flow variables near the wall and is the likely cause for the discrepancies between the numerical and experimental wall pressure distributions.

Cases 2–4: $\delta = 1$ mm

The three cases presented here have inflow conditions of $M_\infty = 3.84$, $P_t = 1.28e + 06$ Pa, and $T_t = 297.6$ K. The freestream Reynolds number for all three cases was computed as $2e + 07$ per meter. Nitrogen is injected at Mach 1 into the test section normal to the surface at a total pressure and temperature of $0.195e + 06$ Pa and 297.6 K, respectively, through an orifice 1-mm wide. A fully developed turbulent profile is imposed at the inflow boundary ($x_1 = 0.05$ m in Fig. 4) as in case 1. Experimental results used for comparisons were taken from the work of Aso et al.[6]

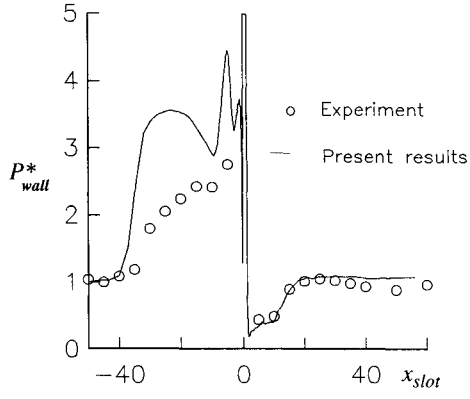

Fig. 14 Surface pressure distribution for case 3.

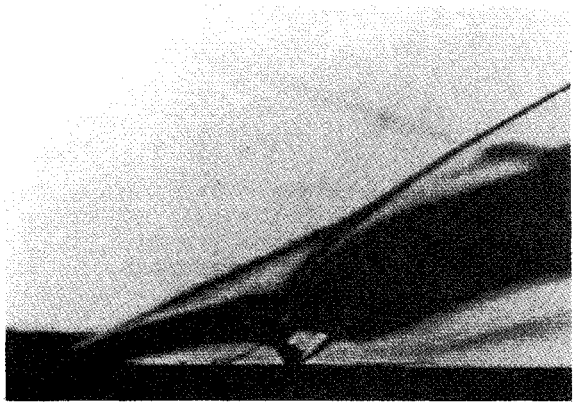

Fig. 15 Experimental schlieren photograph for case 4.

Fig. 16 Numerical schlieren for case 4.

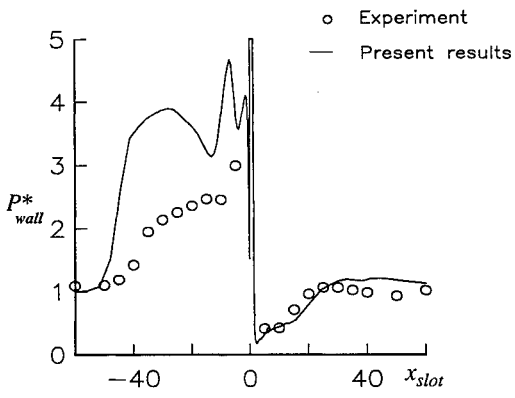

Fig. 17 Surface pressure distribution for case 4.

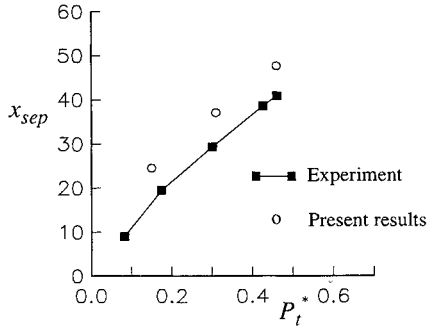

Fig. 18 Separation length as a function of total pressure ratio.

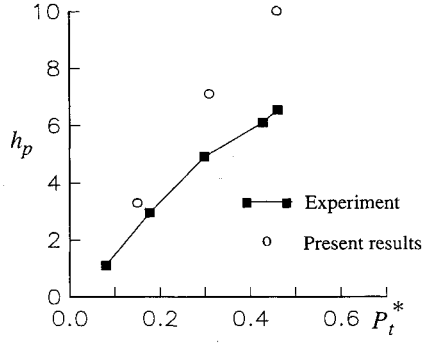

Fig. 19 Penetration height as a function of total pressure ratio.

The initial grid utilized for case 2 (as well as for cases 3 and 4) is similar to that used for case 1. The finite difference grid is adapted at regular intervals with Mach number and density gradients as the primary refinement indicators. The schlieren photograph for case 2 (Fig. 11) is compared with the numerical schlieren of Fig. 12. The main flow features are well represented by the computational procedure with the separation region and the separation shock clearly evident in the numerical schlieren.

Pressure distribution along the wall surface is compared with experimental measurements in Fig. 13. Results obtained from the numerical procedure overpredict the pressure levels ahead of the injection location. Downstream of the slot, the drip in surface pressure from expansion and the recovery caused by the weak recompression shock are well represented by the present calculations. The separation length is also well predicted by the computational procedure.

The injection of N_2 for case 3 is at a total pressure of 0.395e + 06 Pa (P^*_{inj} = 19.7) and a total temperature of 297.6 K. A comparison of the surface pressure distribution with experimental measurements appears in Fig. 14. The increased injection pressure causes stronger pressure peaks ahead of the injection station and enhances the extent of separation regions ahead of and behind the slot. The deviation between experimental and numerical wall pressure levels in the upstream separation region is much more pronounced when compared with the preceding case. At stations downstream of the injection location, experimental and numerical pressure distributions compare quite well.

Nitrogen is injected at a total pressure of 0.595e + 06 Pa for case 4; the total temperature is unchanged from the two preceding cases. The location of the slot is moved downstream (x_1 = 0.06 m in Fig. 4) to enable the shock that results from the interaction between the separation and induced shocks to exit the numerical domain through the outflow boundary. Repeated adaptations are performed, and the experimental schlieren photograph for case 4 (Fig. 15) is compared with the numerical schlieren in Fig. 16. As the injection pressure increases, the strength of the bow shock is enhanced and separation and reattachment regions are significantly enlarged. The extent of the barrel-shaped shear layers, the location of the separation shock, and the size of the Mach disk are magnified when compared with case 2. The upstream migration of the separation location as injection pressures increase is clearly evident when the schlieren photographs of Figs. 11 and 15 or the numerical schlieren plots of Figs. 12 and 16 are compared. The surface pressure distribution in Fig. 17 indicates the presence of spurious pressure oscillations as the flow approaches the injection location, which are absent in the experimental measurements.

A recent paper by Rizzetta[14] indicates that the discrepancies in surface pressure distributions that occur between the experimental measurements and computational results ahead of the injection location may be caused by three-dimensional effects present in the experimental setup. Flow spillage from spanwise locations may produce a relieving effect that reduces the pressure levels upstream of the injection slot. This relief is enhanced at higher pressure levels and larger slot widths.

Two parameters that are indicative of the extent of interaction between the injection and the freestream are the separation length x_{sep} and the penetration height h_p, which indicates the height of the Mach disk. The separation length, which is measured from the slot in the upstream direction, is defined as the x location where the separation shock would hit the wall in the absence of the boundary layer. Values of x_{sep} are plotted for various values of P_{inj}/P_∞ for a slot width of 1 mm; these values are compared with the experimental observations of Aso et al.[6] in Fig. 18. Reasonable agreement is obtained for the separation length; the numerical procedure yields a considerable overprediction of the extent of separation. The comparison of the penetration height in Fig. 19 indicates that, at higher pressure ratios, the numerical procedure yields a much more invasive Mach disk with stronger barrel-shaped shear layers. At lower pressure ratios, the difference between the location of the experimental Mach surface and the computation prediction of its location is small. The cause for this behavior may be attributed to the relieving effect due to flow spillage detailed previously.

Conclusions

Computational results have been obtained for the sonic injection of nitrogen into a Mach 3.8 freestream in an effort to analyze mixing effects in scramjet combustor environments. A dynamic grid adaptation scheme was incorporated into a MacCormack predictor-corrector procedure to enhance the description of the complex flowfields associated with normal injection.

Injection pressures and slot widths are varied in this numerical study; pressure distributions, separation extents, and penetration heights are compared with experimental data. The computational procedure yields a good representation of the flow physics, as well as reasonable agreement with the experimental measurements for the extent of separation and recirculation regions. The main discrepancy between the experimental and computational results is the consistently higher computed surface pressure values in separation regions ahead of the injection slot. Three-dimensional effects, such as spillage in the experimental setup, as well as the inadequacy of the turbulence models used in the analyses may be factors responsible for the differences.

The results presented in this paper illustrate the capability of the grid adaptation procedure in describing the complex flows associated with fuel injection into a supersonic airstream. The simplicity of the procedure and its low computational costs indicate its promise in detailed analysis of mixing and combustion effects in scramjet combustor environments.

Acknowledgments

The authors are grateful to the Theoretical Flow Physics Branch and the Computational Sciences Branch at NASA Langley Research Center for support through Contract NAS1-19320. The authors wish to thank Y. Yamane of the Isikawajima-Harima Heavy Industries Co., Ltd., for supplying the schlieren photographs and experimental data used in the comparisons.

References

[1]Gaffney, R. L., White, J. A., Girimaji, S. S., and Drummond J. P., "Modeling Turbulent/Chemistry Interactions Using Assumed PDF Methods," AIAA Paper 92-3638, July 1992.

[2]Gaffney, R. L., White, J. A., Girimaji, S. S., and Drummond, J. P., "Modeling Temperature and Species Fluctuations in Turbulent, Reacting Flow," 2nd U.S. National Congress on Computational Mechanics (Washington, DC), Aug. 1993.

[3]Drummond, J. P., "Numerical Investigation of the Perpendicular Injector Flow Field in a Hydrogen Fueled Scramjet," AIAA Paper 79-1482, July 1979.

[4]King, P. S., Thomas, R. H., and Schetz, J. A., "Combined Tangential-Normal Injection into a Supersonic Flow," AIAA Paper 89-0622, Jan. 1989.

[5]Thompson, D. S., "Numerical Solution of a Two-Dimensional Jet in a Supersonic Cross-Flow Using an Upwind Relaxation Scheme," AIAA Paper 89-1869, June 1989.

[6]Aso, S., Okuyama, S., Kawai, M., and Ando, Y., "Experimental Study on Mixing Phenomena in Supersonic Flows with Slot Injection," AIAA Paper 91-0016, Jan. 1991.

[7]Fujimori, T., Kawai, M., Ikeda, H., Ando, Y., Ohmori, Y., Aso, S., and Fukuda, M., "Numerical Prediction of Two- and Three-Dimensional Sonic Gas Transverse Injections into Supersonic Flow," AIAA Paper 91-0415, Jan. 1991.

[8]MacCormack, R. W., "The Effect of Viscosity in Hypervelocity Impact Cratering," AIAA Paper 69-354, April 1969.

[9]Ramakrishnan, R., and Singh, D. J., "A Dynamic Grid Adaptation Procedure for Mixing and Reacting Processes in Scramjet Combustors with Injection," AIAA Paper 93-0355, Jan. 1993.

[10]Baldwin, B., and Lomax, H., "Thin-Layer Approximation and Algebraic Model for Separated Turbulent Flows," AIAA Paper 78-257, Jan. 1978.

[11]Drummond. J. P., Rogers, R. C., and Hussaini, M. Y., "A Detailed Numerical Model of a Supersonic Reacting Mixing Layer," AIAA Paper 86-1427, June 1986.

[12]Benson, R., and McRae, D., "A Three-Dimensional Dynamic Solution-Adaptive Mesh Algorithm" AIAA Paper 90-1566, June 1990.

[13]Ramakrishnan, R., "Numerical Simulation of Aerothermal Loads in Hypersonic Engine Inlets Due to Shock Impingement," *Proceedings of the 10th AIAA Applied Aerodynamics Conference*, Pt. 1, AIAA, Washington, DC, 1992, pp. 61–71.

[14]Rizzetta, D. P., "Numerical Simulation of Slot Injection into a Turbulent Supersonic Stream," *AIAA Journal*, Vol. 30, No. 10, 1992, pp. 2434–2439.